Surrogate-Based Optimization of Functionally Graded Plates under Thermo-Mechanical Loading

Igor L. Passos[1], Leonardo G. Ribeiro[1], Evandro Parente Jr.[1], A. Macário C. de Melo[1]

[1]*Departamento de Engenharia Estrutural e Construção Civil, Universidade Federal do Ceará*
Campus do Pici, Bloco 728, 60440-900, Ceará-Brazil
igorlirap@gmail.com.br, leonardoribeiro@alu.ufc.br, evandro@ufc.br, macario@ufc.br

Abstract. Efficient designs for a Functionally Graded Plates (FGP) can be defined via structural optimization. Usually, bio-inspired algorithms are employed in order to carry out the optimization process. However, when analyses are very time-demanding, the process may be too costly, since hundreds or even thousands of analyses may be required. In this work, Sequential Approximate Optimization is employed to provide a more efficient approach. This paper focuses on the maximization of buckling temperature of a ceramic-metal FGP. B-Splines are used to define a continuous material gradation along the thickness direction. Effective material properties are evaluated by the rule of mixtures. The Particle Swarm Optimization (PSO) is applied for structural optimization and Isogeometric Analysis (IGA) is employed to evaluate the structural responses. Then, Sequential Approximate Optimization (SAO) is carried out to reduce the computational cost using Kriging to fit an approximate response surface. A comparison between conventional optimization and SAO is performed, and results show that SAO achieved the optimum design much earlier the conventional approach, requiring fewer high-fidelity evaluations.

Keywords: Functionally Graded Materials, Bio-inspired algorithms, Surrogate Modeling.

1 Introduction

Functionally Graded Materials (FGMs) are a class of smart composite materials which have been gaining interest in various industries, such as aerospacial, biomedical and energy. Under thermo-mechanical loadings, FGMs present a better performance than traditional composites since failure modes such as debonding and delamination do not occur [1].

This work studies ceramic-metal Functionally Graded Plates (FGPs) where the material changes smoothly through the thickness direction from a ceramic, which presents high stiffness and low thermal conductivity, to a metal, which presents better ductility and toughness. To fully explore the benefits of these FGPs, the material gradation can be defined by different methods, such as Power-law and B-Spline functions, to achieve the optimum design for a desired structural behavior.

Bio-inspired algorithms, such as the Particle Swarm Optimization (PSO), are commonly employed for solving structural optimization problems since no gradient information is required. Indeed, many researchers make use of the PSO to optimize FG structures with great success [2, 3]. However, these algorithms often need to perform hundreds or even thousands of function evaluations, which are a major hindrance when numerical methods, e.g. Finite Element Method (FEM) and Isogeometric Analysis (IGA), are employed in the structural analysis.

To reduce the computational cost, Sequential Approximation Optimization (SAO) can be performed, where a costly function is approximated by a surrogate model. New sampling points are then added in regions of interest to improve the model accuracy in promising regions of the design space. This paper aims to perform SAO for FGPs subjected to thermo-mechanical loadings, comparing this approach with the conventional optimization based on the use of numerical methods to evaluate the structural responses. Structural analyses will be performed using IGA. Kriging will be used to fit an approximate response surface, and new data points will be defined via the maximization of the Expected Improvement (EI). Results will be compared in terms of accuracy and computational efficiency.

The rest of the paper is organized as follows. In Section 2, the FGPs are described. In Section 3, PSO and

its parameters are introduced. In section 4, the SAO approach is presented, and surrogate model building and assessment of the EI are discussed. The results and conclusions are presented in Sections 5 and 6, respectively.

2 Functionally Graded Plates

On Functionally Graded Plates, the material composition smoothly changes in the structure's domain. To enhance design flexibility, a B-Spline will be employed to define the gradation along the thickness direction [3, 4]:

$$V_c(\xi) = \sum_{i=1}^{n} B_{i,p}(\xi) V_{c,i} \ , \quad V_m(\xi) = 1 - V_c(\xi) \ , \quad \xi \in [0,1] \tag{1}$$

where $B_{i,p}$ corresponds to B-Spline bases, p is the bases' degree, n is the number of control points, and $V_{c,i}$ is the volume fraction for the i-th control point. B-splines bases are defined recursively using the Cox-de Boor formula based on a knot vector [ξ_1, ξ_2, ..., ξ_{n+p+1}] [3, 4].

Rule of mixtures is a very popular method to find equivalent material properties for the FGP [1]:

$$P = P_c \, V_c + P_m \, V_m \tag{2}$$

where P represents an effective material properties (e.g. the Young's modulus), and P_c and P_m are the properties of ceramic and metal constituents, respectively. Due to its simplicity and popularity, the present work will make use of this approach.

Since FGP can be subjected to a large temperature range, properties are assumed as temperature-dependent for a more accurate model. Touloukian's equation [5] uses P_i unique material coefficients to evaluate the material property P_f at a temperature T:

$$P_f = P_0(P_{-1}T^{-1} + 1 + P_1 T + P_2 T^2 + P_3 T^3) \tag{3}$$

When considering thermal effects, the stresses ($\boldsymbol{\sigma}$) can be computed from [6]:

$$\boldsymbol{\sigma} = \boldsymbol{Q}(\boldsymbol{\varepsilon} - \boldsymbol{\varepsilon}^{th}), \text{ with } \boldsymbol{\varepsilon}^{th} = [\alpha\Delta T, \alpha\Delta T, \alpha\Delta T, 0, 0, 0]^T \tag{4}$$

where $\boldsymbol{\varepsilon}$ and $\boldsymbol{\varepsilon}^{th}$ are the total elastic and thermal strain vectors, α is the thermal expansion coefficient, ΔT is the temperature change and $\mathbf{Q}$ is the elastic constitutive matrix. For a clamped FGP under thermal loading, displacement constraints cause compressive stresses. As a consequence, thermal buckling occurs once a critical temperature ΔT_{cr} is reached. Figure 1 depicts a clamped plate subjected to its critical temperature, considering a uniform temperature distribution.

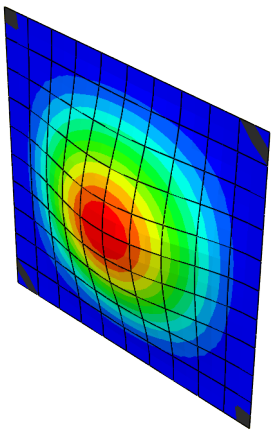

Figure 1. Critical thermal buckling mode

3 Particle Swarm Optimization

Particle Swarm Optimization is a stochastic meta-heuristic optimization algorithm initially developed by Kennedy and Eberhart [7]. The algorithm starts by generating a set of particles at random within the design space.

Each particle j has a position $\mathbf{x}_j^{(i)}$ and a velocity $\mathbf{v}_j^{(i)}$, which guides the particle towards a possible optimum. The superscript i denotes the current iteration. These vectors are iteratively updated by:

$$\mathbf{x}_j^{(i+1)} = \mathbf{x}_j^{(i)} + \mathbf{v}_j^{(i+1)}, \quad \text{where} \quad \mathbf{v}_j^{(i+1)} = w\mathbf{v}_j^{i} + c_1 r_1(\mathbf{x}_{p,j}^{(i)} - \mathbf{x}_j^{(i)}) + c_2 r_2(\mathbf{x}_{g,j}^{(i)} - \mathbf{x}_j^{(i)}) \tag{5}$$

where r_1 and r_2 are random numbers in the range $[0, 1]$, $\mathbf{x}_{p,j}^{(i)}$ is the best position the particle has visited, and $\mathbf{x}_{g,j}^{(i)}$ is the best location ever visited by the swarm. The control parameters for this algorithm are the particle's inertia w and the cognitive and social factors c_1 and c_1, Unfeasible designs are penalized using an exterior penalty approach. The swarm evolves into new generations until a stopping criterion is met, which may be related to a number of stall generations (G_{stall}) or a maximum number of generations (G_{max}).

To further improve PSO exploration capabilities, Barroso et al. [8] proposed the use of a mutation operator. Once a new position $\mathbf{x}_j$ is calculated at the i-th iteration, each variable $x_{j,k}^{(i)}$ has a probability p_{mut} of mutating to a new value inside the bound constraints.

4 Sequential Approximate Optimization

Conventional optimization based on the evaluation of structural responses via numerical methods may become very costly when hundreds of even thousands of design evaluations are required. To provide an efficient optimization process, one may use Sequential Approximate Optimization (SAO). Based on a few high-fidelity responses (evaluated by FEM or IGA), a surrogate model of a costly function is fitted, and used to guide in the optimization process. New sampling points are then added, based on a chosen infill criterion [9, 10], to improve the surrogate accuracy in promising regions of the design space.

In these cases, model performance is a function of the selected sampling points. First, the number of sampling points is often defined based on the number of variables. In this work, different sample sizes will be tried out. Initially, since no information about the function behavior is known, sampling points should be selected in a way to ensure the coverage of the design space [9]. Thus, the location of these points is defined using a Design of Experiments (DoE) technique, such as the Latin Hypercube Sampling. This is an stochastic sampling technique, and, to guarantee that the design is uniform, 20 different samples are generated, and the one where the minimum distance between two points is maximized is selected to perform the model building [4].

After evaluation of the sampling points, a Kriging model is fitted, and is then used to guide the further selection of new data points. This should be biased toward regions where the model is expected to improve upon the optimum design, and should try to balance *exploitation* and *exploration* [10, 11]. These aspects will be further described in the following sections.

4.1 Kriging

The Kriging model was first proposed by Krige [12], but was brougth to engineering design by Sacks et al. [13]. In its general form, the model can be seen as the sum between a global trend $g(\mathbf{x})$ and its autocorrelated localized deviations $Z(\mathbf{x})$:

$$\hat{y}(\mathbf{x}) = g(\mathbf{x}) + Z(\mathbf{x}) \tag{6}$$

For different types of Kriging, $g(\mathbf{x})$ may assume different forms. In its most popular version, the Ordinary Kriging, the global trend is given by a constant term μ. The localized deviations are assumed to be the realization of a stochastic process with mean zero and covariance.

$$\text{cov}(\mathbf{y}, \mathbf{y}) = \sigma^2 \, \mathbf{\Psi} \tag{7}$$

where σ^2 is the process variance and $\mathbf{\Psi}$ is a correlation matrix, where $\Psi_{ij} = \text{cor}[y_i, y_j]$. The correlation between two responses is drawn using an appropriate similarity-based kernel, such as the Gaussian:

$$\text{cor}\left[y_i, y_j\right] = \exp\left(-\sum_{k=1}^{m} \theta_k \left|x_{i,k} - x_{j,k}\right|^{p_k}\right) \tag{8}$$

The fitting of the Kriging model involves the definition of μ, σ^2, θ_k, and p_k. These can be defined by their Maximum Likelihood Estimators (MLE). To that end, the $\ln$-likelihood function is given by:

$$\ln L = -\frac{n}{2} \ln\left(2\,\pi\right) - \frac{n}{2} \ln\left(\sigma^2\right) - \frac{1}{2} \ln\left|\mathbf{\Psi}\right| - \frac{\left(\mathbf{y} - \mathbf{1}\,\mu\right)^T \mathbf{\Psi}^{-1} \left(\mathbf{y} - \mathbf{1}\,\mu\right)}{2\,\sigma^2} \tag{9}$$

by differentiating in terms of μ and σ^2 and equating to zero, one finds the MLE for the mean and the variance:

$$\hat{\mu} = \frac{\mathbf{1}^T \boldsymbol{\Psi}^{-1} \mathbf{y}}{\mathbf{1}^T \boldsymbol{\Psi}^{-1} \mathbf{1}}, \text{ and } \hat{\sigma}^2 = \frac{(\mathbf{y} - \mathbf{1}\hat{\mu})^T \boldsymbol{\Psi}^{-1} (\mathbf{y} - \mathbf{1}\hat{\mu})}{n} \tag{10}$$

The concentrated ln-likelihood function is obtained by replacing the estimators of Eq. (10) into (9) and removing the constant terms:

$$\ln L \approx -\frac{n}{2} \ln(\hat{\sigma}^2) - \frac{1}{2} \ln |\boldsymbol{\Psi}| \tag{11}$$

Unfortunately, the hyper-parameters (p_k and θ_k) can not be found by the same analytical procedure. For simplification purposes, we adopt $p_k = 2.0$. Then, the definition of θ_k comes from the solution of the following optimization problem:

$$\begin{cases} \text{minimize} & -\ln L(\boldsymbol{\theta}) \\ \text{where} & \boldsymbol{\theta}_L \leq \boldsymbol{\theta} \leq \boldsymbol{\theta}_U \end{cases} \tag{12}$$

Finally, after all parameters have been set, the Kriging model prediction is given by [9]:

$$\hat{y}(\mathbf{x}) = \hat{\mu} + \boldsymbol{\psi}^T \, \boldsymbol{\Psi}^{-1} \, (\mathbf{y} - \mathbf{1} \, \hat{\mu}) \tag{13}$$

4.2 Infill criteria

In SAO, the selection of new points should consider *exploitation*, related to regions where the model prediction is minimized, and *exploration*, related to regions where the model uncertainty is higher. The Kriging model has a very nice way to quantify model uncertainty by the evaluation of its posterior variance [14]:

$$\hat{s}^2(\mathbf{x}) = \sigma^2 \left(1 - \boldsymbol{\psi}^T \boldsymbol{\Psi}^{-1} \boldsymbol{\psi}\right) \tag{14}$$

Figure 2 shows the confidence interval ($\hat{y} \pm \hat{s}$) for the Kriging prediction considering a one-dimensional function. At the sampling points, since there is no uncertainty regarding their true response, $\hat{s}(x) = 0$. However, $\hat{s}(x)$ increases as x gets farther from the sampling points.

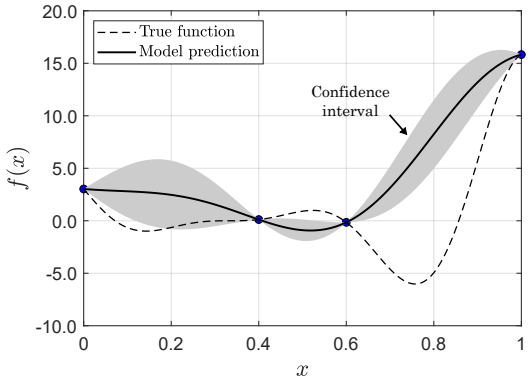

Figure 2. Kriging confidence interval for a one-dimensional function.

The location of new sampling points is often defined by the optimization of a chosen acquisition function. To balance exploitation and exploration, the addition of the point that maximizes the Expected Improvement (EI) can be performed [10]. The EI is given by:

$$E[I(\mathbf{x})] = (y_{min} - \hat{y}(\mathbf{x})) \, \frac{1}{2} \left[1 + \text{erf}\left(\frac{y_{min} - \hat{y}(\mathbf{x})}{\hat{s}\sqrt{2}}\right)\right] + \hat{s} \, \frac{1}{\sqrt{2\pi}} \exp\left[-\frac{1}{2}\left(\frac{y_{min} - \hat{y}(\mathbf{x})}{\hat{s}}\right)^2\right] \tag{15}$$

Figure 3 presents how the criterion behaves for subsequent iterations. In the second iteration, the criterion is able to select a point near the region of the global optimum. The global optimum is then found at the third iteration. For problems with cheap constraints, these can be evaluated and, if a candidate solution is unfeasible, its EI is set to zero.

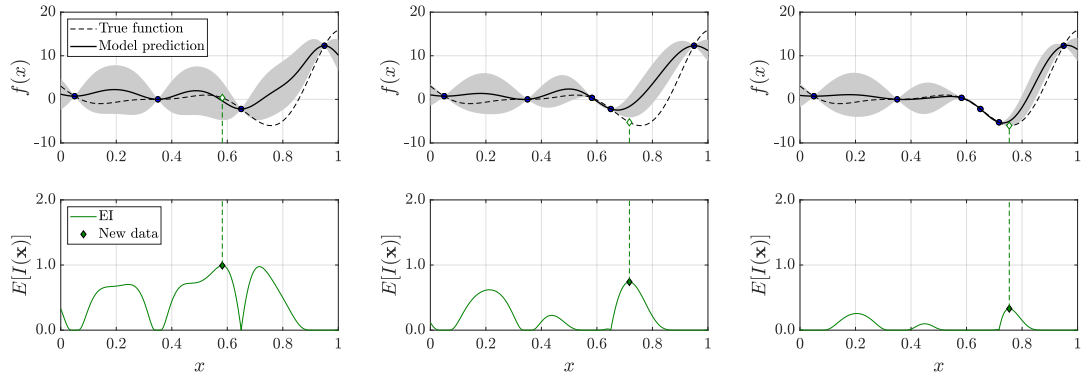

(a) Iteration 1 (b) Iteration 2 (c) Iteration 3

Figure 3. Improvement of the model using the EI criterion.

5 Numerical example

The optimization of a clamped square FGP ($a = b = 1$ m, $a/h = 100$) is performed. Silicon nitride (Si_3N_4) is used as a ceramic material alongside stainless steel (SUS304) as a metal. Both of their properties are presented in Table 1. Effective properties are defined via the rule of mixtures as shown in Eq. (2). It is assumed that material gradation along the thickness direction is symmetrical at mid-plane. Gradation is defined by a B-Spline using 9 control points, but, due to symmetry regarding the mid-plane, there are only 5 design variables.

Table 1. Material properties for T_{ref} = 300 K

Material	α [K^{-1}]	E [GPa]	υ	ρ [kg/m^3]
SUS304	15.32×10^{-6}	207.79	0.30	8000
Si_3N_4	7.474×10^{-6}	322.27	0.30	2730

The plate is subjected to a uniform temperature distribution $T_{\text{ref}} = 300$ K. The objective is to maximize the critical temperature. Silicon nitride and stainless steel are assumed to cost $C_c = 50$ USD/kg and $C_m = 3$ USD/kg respectively [15], making the plate's price range $[240, 1185]$ USD. It is then imposed a maximum cost of $C_t = 600$ USD. This problem can be expressed as:

$$\begin{cases} \text{Maximize} & \Delta T_{cr}(\mathbf{x}), \text{ where } \mathbf{x} = (x_1, x_2, \ldots, x_5) \\ \text{Subjected to} & C_c\rho_c \dfrac{1}{h}\int_{-h/2}^{h/2} V_c dz + C_m\rho_m \dfrac{1}{h}\int_{-h/2}^{h/2} V_m dz \leq C_t \end{cases} \tag{16}$$

The performance of the optimization algorithms is evaluated in terms of Normalized Root Mean Squared Error (NRMSE), Wall-Clock Time (WCT), and Number of Evaluations (NE). A total of 10 runs is performed for each case study and the average results ($\overline{\text{NRMSE}}$, $\overline{\text{WCT}}$, $\overline{\text{NE}}$) are then calculated. For conventional optimization using PSO, $\overline{\text{NE}}$ represents the average number of high-fidelity sampling points evaluated. For PSO, three population sizes N_p were tried out: 20, 40 and 80. Similarly, for SAO approaches, three different number of initial sampling points N_i were tested: 5, 10 and 20. The stopping criteria adopted were G_{max} = 50 and G_{stall} = 20, and the PSO parameters used were w = 0.7 and $c_1 = c_2$ = 0.15. All numerical simulations were performed on a computer with an I9-9820X, 3.30 GHz clock speed and 128 GB of RAM. No parallel processing was used.

Due to its higher stiffness and lower expansion factor, the ceramic material provides a better response when the plate is subjected to thermal buckling. This way, a homogeneous ceramic plate, with $\mathbf{x} = \mathbf{1}$, presents ΔT_{cr} = 44.81 K, while a fully metallic plate, $\mathbf{x} = \mathbf{0}$, has a ΔT_{cr} = 21.87 K. Therefore, without the cost-related constraint, the optimal design would be a homogeneous ceramic plate. However, considering the cost constraint, the optimum is found at $\mathbf{x}$ = [1.0 1.0 0.5238 0.0 0.0], for which ΔT_{cr} = 32.22 K. Figure 4 describes the optimum design found. The bottom and top surfaces are fully ceramic, and volume fraction varies to fully metallic material towards the mid-plane. The buckling mode is similar to the one shown in Figure 1.

Table 2 presents a performance comparison of conventional and SAO approaches. All optimizations achieved designs fairly close to the global optimum. For conventional optimization (PSO + IGA), the population with 40

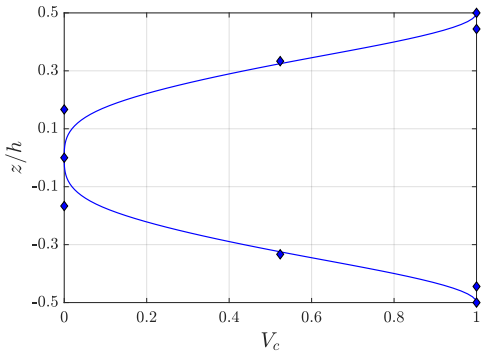

Figure 4. Volume fractions for optimum design

particles achieved the global optimum for all optimizations, but convergence is around 2 times slower compared with the one using N_p = 20.

Table 2. Performance of conventional and SAO approaches

PSO + IGA					SAO				
N_p	$\overline{\Delta T_{\text{cr}}}$	$\overline{\text{NRMSE}}$	$\overline{\text{WCT}}$ (min)	$\overline{\text{NE}}$	N_i	$\overline{\Delta T_{\text{cr}}}$	$\overline{\text{NRMSE}}$	$\overline{\text{WCT}}$ (min)	$\overline{\text{NE}}$
20	32.21	0.01%	16.00	1014	5	32.22	0.00%	1.48	30
40	32.22	0.00%	32.28	2040	10	32.22	0.00%	1.55	32
80	32.22	0.00%	62.71	3952	20	32.22	0.00%	2.39	41

On the other hand, the SAO approaches lead to a faster convergence, as $\overline{\text{WCT}}$ is significantly lower, while also being more accurate, as all the optimizations achieved the global optimum with $\overline{\text{NRMSE}}$ = 0.00%. Moreover, the G_{stall} stopping criterion was met, contrary to the conventional PSO, which performed the maximum number of evaluations for most of the optimizations. The SAO using 5 initial sampling points was the best strategy found, computing only 30 high-fidelity evaluations in total, while still able to find the global optimum. In fact, its $\overline{\text{WCT}}$ was 1.48 minutes, which is around 10 times faster than conventional PSO optimization with 20 particles.

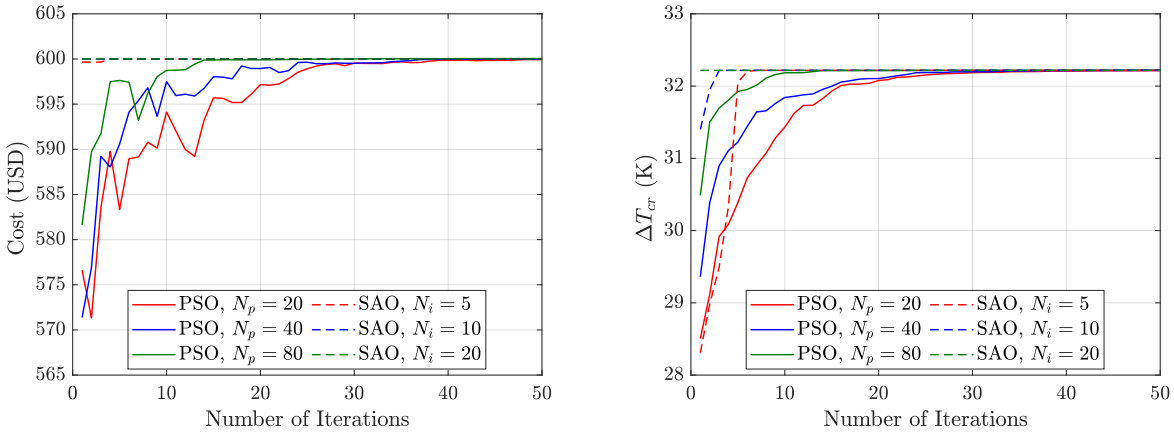

(a) Plate cost over iterations

(b) Objective function over iterations

Figure 5. Convergence of the optimization methods throughout the iterations

Figure 5a depicts how the cost of the best design found changes over iterations. For PSO, each of the 50 iterations involves N_p high-fidelity IGA evaluations. For the SAO approaches, each iteration performs only one high-fidelity IGA evaluation, which is added to the sample. In all cases, the constraint was eventually active, and the cost converged to $C_t = 600$ USD. For $N_p = 20$ and $N_p = 40$, this result was achieved after 30 iterations,

while a faster convergence can be found for $N_p = 80$, where this value was achieved after 15 iterations. On the other hand, the SAO approaches found this value as soon as the first iteration.

Figure 5b then describes the improvement over the best response found throughout the iterations. As expected, the PSO with $N_p = 80$ presents a steeper curve and a faster convergence, although more high-fidelity evaluations were performed. The curves related to the SAO approaches are even steeper, and, for $N_i = 20$, the curve is fairly close to a horizontal line, as the optimum design is found already in the first iteration.

6 Conclusion

In this paper, the maximization of the critical buckling temperature of a Functionally Graded Plate was performed. The Particle Swarm Optimization algorithm was employed considering different population sizes. Overall, all the optimizations achieved results close to the global optimum with great accuracy, presenting a relatively fast convergence, especially for higher values of N_p. However, higher N_p also incur in a higher Wall-Clock Time. The same problem was also solved using Sequential Approximate Optimization, which converged much faster, with a higher accuracy, and with far fewer function evaluations, thus proving to be an excellent strategy to reduce computational cost.

Acknowledgements. The financial support by CNPq (Conselho Nacional de Desenvolvimento Científico e Tecnológico) is gratefully acknowledged.

Authorship statement. The authors hereby confirm that they are the sole liable persons responsible for the authorship of this work, and that all material that has been herein included as part of the present paper is either the property (and authorship) of the authors, or has the permission of the owners to be included here.

References

[1] V. Boggarapu, R. Gujjala, S. Ojha, S. Acharya, P. Venkateswara babu, S. Chowdary, and D. kumar Gara. State of the art in functionally graded materials. *Composite Structures*, vol. 262, pp. 113596, 2021.
[2] M. Ashjari and M. Khoshravan. Mass optimization of functionally graded plate for mechanical loading in the presence of deflection and stress constraints. *Composite Structures*, vol. 110, pp. 118–132, 2013.
[3] D. T. T. Do, D. Lee, and J. Lee. Material optimization of functionally graded plates using deep neural network and modified symbiotic organisms search for eigenvalue problems. *Composites Part B: Engineering*, vol. 159, pp. 300–326, 2019.
[4] L. G. Ribeiro, M. A. Maia, E. Parente Jr.., and A. M. C. D. Melo. Surrogate based optimization of functionally graded plates using radial basis functions. *Composite Structures*, vol. 252, 2020.
[5] P. U. T. P. R. Center and Y. Touloukian. *Thermophysical Properties Research Literature Retrieval Guide: Editor: Y. S. Touloukian*. Number v. 3 in Thermophysical Properties Research Literature Retrieval Guide: Editor: Y. S. Touloukian. Plenum Press, 1967.
[6] J. Reddy. Mechanics of laminated plates and shells theory and analysis. *CRC Press, Boca Raton, FL*, vol. , 2004.
[7] J. Kennedy and R. Eberhart. *Particle swarm optimization*, volume 4. IEEE, 1995.
[8] E. S. Barroso, E. Parente, and A. M. C. Melo. A hybrid PSO-GA algorithm for optimization of laminated composites. *Structural and Multidisciplinary Optimization*, vol. 55, n. 6, pp. 2111–2130, 2017.
[9] A. I. J. Forrester, A. Sobester, and A. J. Keane. *Engineering design via surrogate modelling: a practical guide*. Wiley, 2008.
[10] D. R. Jones, M. Schonlau, and W. J. Welch. Efficient global optimization of expensive black-box functions. *Journal of Global Optimization*, vol. 13, pp. 455–492, 1998.
[11] A. Sobester, S. J. Leary, and A. J. Keane. On the design of optimization strategies based on global response surface approximation models. *Journal of Global Optimization*, vol. 33, pp. 31–59, 2005.
[12] D. G. Krige. A statistical approaches to some basic mine valuation problems on the witwatersrand. *Journal of the Chemical, Metallurgical and Mining Society of South Africa*, vol. 52, pp. 119–139, 1951.
[13] J. Sacks, W. J. Welch, T. J. Mitchell, and H. P. Wynn. Design and analysis of computer experiments. *Statistical Science*, vol. 4, n. 4, pp. 409–423, 1989.
[14] K. P. Murphy. *Machine Learning: A probabilistic perspective*. MIT Press, 2012.
[15] V. Franco Correia, J. S. Moita, F. Moleiro, and C. M. M. Soares. Optimization of Metal–Ceramic Functionally Graded Plates Using the Simulated Annealing Algorithm. *Applied Sciences*, vol. 11, n. 2. Number: 2, 2021.